ACS APPLIED MATERIALS & INTERFACES

Research Article

www.acsami.org

Effect of Substrate Temperature on the Spin Transport Properties in C_{60}-Based Spin Valves

Feng Li*

High Magnetic Field Laboratory, Chinese Academy of Sciences, Hefei 230031, China

ABSTRACT: We report the effect of the substrate temperature on the magnetoresistance (MR) of C_{60}-based spin-valve (SV) devices with the sandwich configuration of $La_{0.67}Sr_{0.33}MnO_3$ (LSMO)/C_{60}/cobalt (Co). The C_{60} interlayer deposited at different substrate temperatures resulted in four types of devices. We observed that all types of devices showed a monotonic increase in their MR ratio with the substrate temperature. Interestingly, an especially large MR (|−28.5%|) was obtained in the device fabricated at a higher substrate temperature, whereas for the other types of devices, the MR magnitudes were about a few percent. On the basis of the $I-V$ measurements as well as SEM and AFM characteristics, we have found that the higher substrate temperature can cause many pits and hollows in the organic film, and these pits will increase the tunneling probability of spin-polarized carriers from one ferromagnetic electrode to the other.

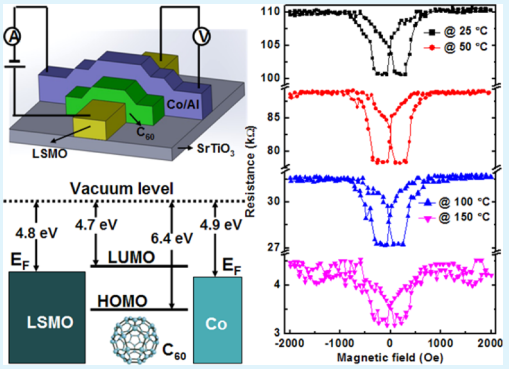

KEYWORDS: *organic spintronics, organic spin valves, magnetoresistance effect, substrate temperature*

INTRODUCTION

Recently, organic semiconductors (OSCs) have become a promising candidate for use as the nonmagnetic spacer in spin-valve (SV) devices, which is motivated by their long spin-relaxation lifetimes resulting from weak spin−orbit and hyperfine interactions.[1,2] A giant magnetoresistance (GMR) effect has been demonstrated for vertical SV devices employing organic spacers, such as tris(8-hydroxyquinoline) aluminum (Alq_3) and rubrene, thicker than 100 nm.[3−7] In parallel, OSC ultrathin layers performed successfully in spin tunnel junctions,[8−10] and extremely high (>300%) tunneling magentoresistance (TMR) has been observed at low temperatures.[9] However, in some cases where a clear GMR effect was reported, the organic SV devices with a relatively thick OSC spacer display low device resistance and a weak temperature dependence of their $I-V$ behavior, which is characteristic of TMR. This fact raised a serious debate on whether the observed MR in the OSV is due to carrier transport within the organic layer or tunneling through the locally thin areas of the OSC layer.[11−13] It was found that interfacial reaction and metal penetration into the 'soft' organic layer takes place upon the deposition of the ferromagnetic electrode, leading to the formation of an ill-defined layer and pinhole channels within the OSC spacer.[3,14,15] Furthermore, in the most recent experimental works on the organic SV devices,[3−20] the organic interlayer had mostly an amorphous structure.

Fullerene C_{60} was chosen as an organic spacer in the vertical SV devices in our work. This was motivated by its very weak hyperfine interaction resulting from the absence of polarized hydrogen nuclei[16] as well as the good match of the lowest unoccupied molecular orbital (LUMO) of C_{60} with the Fermi energy of common ferromagnetic electrodes, which makes a relatively easy carrier injection from the electrodes. Besides, the C_{60} molecules are very robust, unlike other organic materials, and can be sustained without being damaged upon electrode deposition.[17−20]

Here, by changing the substrate temperature during the deposition of C_{60} film, we have improved the crystallinity of the C_{60} interlayer and have fabricated different LSMO/C_{60}/Co devices that exhibit diverse MR values with the same C_{60} thickness. Furthermore,on the basis of the $I-V$ measurements as well as SEM and AFM characteristics, we have obtained clear evidence of the spin transport behavior in these devices.

EXPERIMENTAL SECTION

The device structure is shown schematically in Figure 1a. The 100 nm thick and ∼1 mm wide LSMO films, which are half-metallic ferromagnets with a nearly 100% spin polarization that are also very stable, were deposited on $SrTiO_3$ (STO) ⟨100⟩ substrates using a pulsed-laser deposition method through a shadow mask. After cleaning using acetone, the substrate with the narrow LSMO film was introduced into the evaporation chamber (base pressure of $\lesssim 1 \times 10^{-7}$ Torr) where a C_{60} layer was thermally evaporated. The 80 nm thick C_{60} film was vacuum evaporated at the same evaporation rate, confirmed by the thickness profilometer, but at different substrate temperatures (25, 50, 100, and 150 °C, respectively). The growth rate and total thicknesses of the C_{60} interlayer in the four sets of devices were set to the same value and in situ monitored by a quartz crystal thickness monitor. Finally, the 10 nm thick Co film was thermally evaporated as the top ferromagnetic electrode and subsequently capped with a 30 nm Al-protection layer using a shadow mask. The cross-bar junction area was about 0.5 × 1 mm^2. All fabrication steps

Received: June 5, 2013
Accepted: July 29, 2013
Published: July 29, 2013

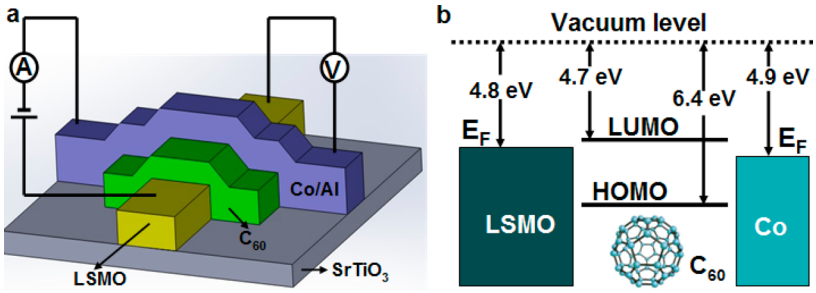

Figure 1. (a) Schematic diagram of our spin-valve-device structure with an $SrTiO_3$ substrate/$La_{0.67}Sr_{0.33}MnO_3$/C_{60}/Co/Al. (b) Schematic band diagram of the organic device showing the Fermi levels (E_F), the work functions of the two ferromagnetic electrodes ($La_{0.67}Sr_{0.33}MnO_3$ and Co), and the highest occupied molecular orbital (HOMO) and lowest unoccupied molecular orbital (LUMO) levels of C_{60}.

involving the organic layer and the top electrode were performed inside a glovebox or inside the glovebox-integrated vacuum evaporator.

The crystalline phase of the C_{60} films was identified by X-ray diffraction (XRD) using the Rigaku-TTR3 X-ray diffractometer with Cu Kα (λ = 1.5406 Å) radiation. The morphology of the samples was determined by field-emission scanning electron microscopy (FESEM) (FEI, Model Sirion-200). The morphology of the C_{60} layer was characterized with a Veeco MultiMode (NanoScope V) AFM in tapping mode. The MR measurements were performed using the standard four-probe method in a Quantum Design Physical Property Measurement System (PPMS) under an external in-plane magnetic field. The MR value is defined by the expression MR = $(R_{AP} - R_P)/R_P \times 100\%$, where R_{AP} and R_P are the resistances of the antiparallel and parallel magnetization configurations of two electrodes, respectively. Figure 1a also shows the experimental set up for a four-probe measurement. I–V measurements for two ferromagnetic electrodes in a parallel configuration were performed using a Keithley 2612 source measure unit, with the positive pole connected to the LSMO electrode. Furthermore, the energetic location of the highest occupied molecular orbital (HOMO) and lowest unoccupied molecular orbital (LUMO) of C_{60} together with the Fermi levels (E_F) and the work functions of LSMO and Co[3,19] are shown in Figure 1b, which indicate the good match of the LUMO of C_{60} with E_F of common ferromagnetic electrodes, making a relatively easy carrier injection from the electrodes. The inset shows the chemical structure of C_{60}.

RESULTS AND DISCUSSION

The inset of Figure 2a shows a typical MR trace measured in a LSMO/C_{60} (80 nm)/Co spin-valve device at 50 K in which the C_{60} interlayer was deposited at a substrate temperature of 25 °C. The figure shows that a sizable MR can be achieved in these devices. The main panel of this figure shows that the magnitude of the MR signal decreases with increasing temperature. Furthermore, we can see that all of the devices show a typical negative MR loop, which is in accordance with previous reports on organic spin-valve devices employing LSMO and Co as the electrodes.[3−5,19] The temperature dependence is believed to reflect a loss in the spin-injection efficiency from the LSMO.[19] Figure 2b shows the bias-voltage dependence of the MR ratio at 50 K for the SV device prepared at a substrate temperature of 25 °C. The asymmetric magnetoresistance ratio for the bias voltage is due to different electrodes (LSMO and Co), which is similar to previous reports.[3−5,11,13]

Figure 3a shows the typical MR curves for the organic SV devices, measured at 50 K, with the 80 nm thick C_{60} interlayers prepared at substrate temperatures of 25, 50, 100, and 150 °C, respectively. The resistance of the devices decreases monotonously with the substrate temperature. For the SV device fabricated at a substrate temperature of 25 °C, the resistance is more than 100 kΩ, whereas for the device fabricated at a substrate temperature of 150 °C, its resistance exhibits only a

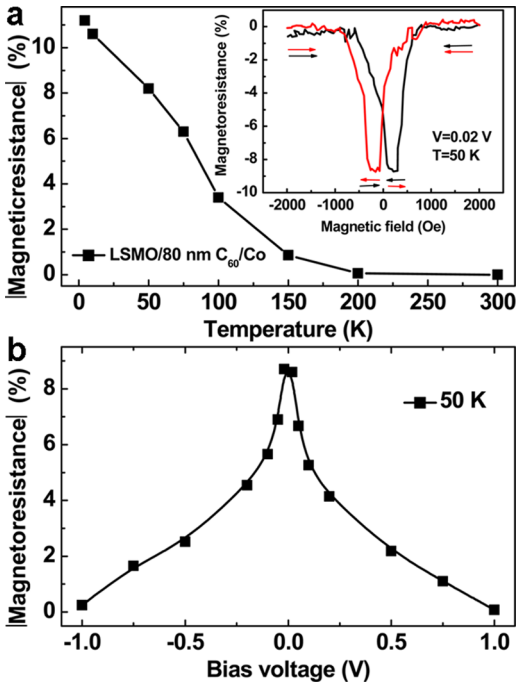

Figure 2. (a) Temperature dependence of the magnitude of magnetoresistance measured in the organic spin valve with an 80 nm thick C_{60} interlayer. The inset shows the magnetoresistance at 50 K. (b) Bias-voltage dependence of the magnitude of magnetoresistance for the organic spin valve measured at 50 K.

few kilo-ohms. It is very interesting that the organic spin-valve devices with the same thick organic interlayer deposited at different substrate temperatures exhibit such large differences in their resistance. Furthermore, because the fabricated C_{60}-based SV devices show the junction resistance larger than 1000 Ω, which is two orders of magnitude higher than that of the LMSO and Co electrode, the MR signal should not be associated with an anisotropic magnetoresistance effect in the LMSO and Co electrode.

The MR ratios, calculated on the basis of the resistances of the devices that were prepared at four substrate temperatures in Figure 3a, versus the magnetic field (H) at 50 K are shown in Figure 3b, which are 8.6, 11.2, 13.3, and 27.6% for the devices fabricated at substrate temperatures of 25, 50, 100, and 150 °C, respectively. From Figure 3b, it is observed that the magnitude of the MR ratios increases moderately with the increasing substrate temperature from 25 to 100 °C, whereas at a substrate temperature of 150 °C, the magnitude of the MR ratio increases intensely. To investigate further the relationship

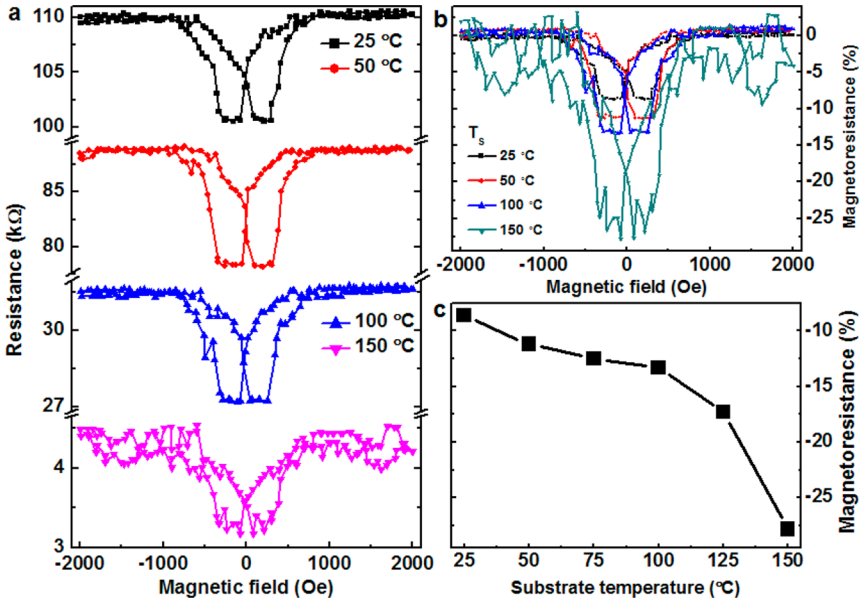

Figure 3. (a) Magnetoresistance curves of our spin-valve devices at 50 K, which were prepared at different substrate temperatures. (b) Magnetoresistance ratios for the devices in panel a. (c) Substrate temperature dependence of the magnetoresistance ratio.

between the MR ratio and the substrate temperature, we fabricated the SV devices with the same thick organic interlayer of 80 nm at additional different substrate temperatures and measured the MR ratios at 50 K. Figure 3c shows that the magnitude of the MR signal increases with increasing substrate temperature. Furthermore, it can be seen clearly that the MR ratio of the device prepared at a substrate temperature of 150 °C is extraordinarily larger than that of the devices that were fabricated at other substrate temperatures. It is a very fascinating physical phenomenon. We deduce tentatively that it may originate from a high crystallinity of the C_{60} interlayer fabricated at a high substrate temperature, especially at 150 °C. This is because the high crastallinity is propitious to the transport of the spin polarized carriers; thus, the spin-relaxation length is very long in high crystalline materials.

To clarify further the reason for the large MR ratio in the device prepared at a high substrate temperature, we have performed specular X-ray diffraction (XRD) measurements to determine the crystal structure, and we have investigated the structural change with the substrate temperature. The specular XRD patterns of the C_{60} films, deposited on STO/LSMO at four different substrate temperatures to mimic their growth as in the actual spin-valve devices, are shown in Figure 4. It can be seen that the XRD pattern of a C_{60} thin film displays strong

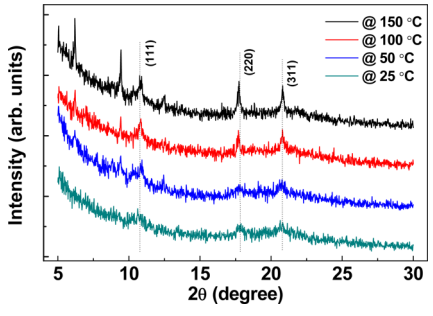

Figure 4. X-ray diffraction patterns for the C_{60} films grown on LSMO at different substrate temperatures.

peaks that correspond to the (111) and (311) reflections of the face-centered cubic (fcc) phase of C_{60}, revealing the crystalline nature of the sample. Every corresponding diffraction peak of the films, prepared at different substrate temperatures, appear at the same degree, which means that the crystal structure of the four films is similar. However, we found that the corresponding diffraction peaks are very weak for the C_{60} film fabricated at a substrate temperature of 25 °C. It should also be noted that the diffraction peaks become stronger gradually as the substrate temperature increases and the diffraction peaks for the film prepared at a substrate temperature of 150 °C are particularly stronger than those of other films prepared at the lower substrate temperatures. This verifies preliminarily that the large MR ratio measured in the device prepared at a high substrate temperature could arise from high crystallinity for the C_{60} interlayer deposited at a high substrate temperature and that crystallinity generally favors an enhancement in mobility.

To gain deeper insight into the mechanism of spin transport in C_{60}-based spin valves with an 80 nm C_{60} interlayer of different crystalline degrees, current−voltage (I−V) characteristics for two ferromagnetic electrodes in a parallel configuration of the SV devices with the same C_{60} thicknesses deposited at different substrate temperatures were measured at different temperatures and studied, as shown in Figure 5. For the device grown at a substrate temperature of 150 °C, the behavior of the I−V curves are shown in Figure 5a. It is shown that I−V curves are weakly nonlinear and are almost temperature independent, which indicates the evident characteristic of spin-polarized carrier tunneling.

Spin-polarized carrier transport can be usually described as a sum of two distinct pathways: one is the tunneling through the HOMO−LUMO gap and the other is the electron injection and hopping transport within the LUMO levels. The elastic tunneling through the barrier is generally considered to be limited to 2 to 3 nm of the insulator.[21] At a small thickness of the organic semiconductor spacer, the multistep tunneling current through the defect states inside the gap will serves as the main channel of the device current because of the existence of an injection barrier at the Co/C_{60} interface. Beyond the

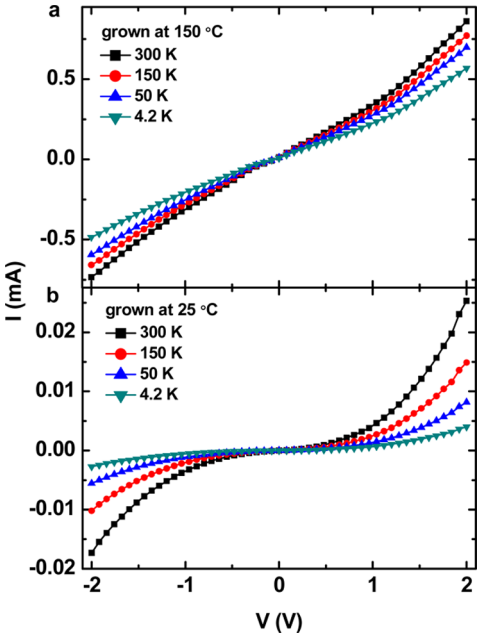

Figure 5. *I*–*V* curves for LSMO and Co in a parallel configuration measured at different temperatures for the LSMO/C_{60}/Co spin valves with the 80 nm C_{60} layer that were fabricated at a substrate temperature of (a) 150 and (b) 25 °C.

tunneling limit, electrons have to be elevated thermally or via the electric field to the LUMO level,[11] where electrons can hop more easily among the LUMO levels of adjacent molecules. Thus, the current will be controlled by carrier injection and transport within the C_{60} layer.

For the C_{60} film that we prepared with a thickness of ~80 nm, spin-polarized carrier tunneling should be unlikely to occur in such a thick organic interlayer. Furthermore, it is worth noting from Figure 5a that the device resistances, measured at four different temperatures, for the device prepared at a substrate temperature of 150 °C are on the order of several thousand ohms, which is about two orders of magnitude lower than those for the device prepared at a substrate temperature of 25 °C. The behavior of the *I*–*V* characteristics for the device prepared at a substrate temperature of 25 °C are shown in Figure 5b, which are strikingly different. It is shown that the *I*–*V* curves have now become largely temperature dependent and strongly nonlinear at low temperatures. In light of the criteria for distinguishing tunneling and spin injection,[11,12] these kinds of *I*–*V* curves together with the observation of MR feature is obviously indicative of spin-polarized injection. Therefore, it should be an unintelligible puzzle as to why the mechanism of the spin-polarized transport is so different in the devices with the same thickness of the C_{60} interlayer. In light of the above experimental results and the corresponding analysis, we deduce that the significantly larger spin-dependent transport length in the organic interlayer with high crystallinity would not be regarded as the dominate factor to achieve the exceptionally larger value of the MR ratio in the device that was prepared at a substrate temperature of 150 °C.

Generally, it should be pointed out that highly crystalline structures in the film will form many large crystals at the surface of the film and will increase the surface roughness of the film. Although for the film with the amorphous-like structure and low crystallinity, it will display a relatively homogeneous surface morphology. Large crystals on the surface of the film will potentially lead to pinholes and pits in the vertical devices. The presence of pinholes and pits in the vertical device will increase the possibility of pinhole channels and magnetic metallic impurities within the organic interlayer, resulting from the penetration of metallic atoms into the pits of the organic film during magnetic metallic electrode deposition and thereby decrease the effective thickness of the organic spacer and make the effective organic interlayer thickness to be in the range of spin-polarized tunneling. The presence of spin-polarized tunneling channels in the C_{60} spacer should contribute more significantly to the occurrence of the extremely large value of the MR ratio in our organic SV devices. This issue merits further investigation.

On the basis of the above analysis and with a view to gain more insight into the origin of the large value of MR ratio, we performed SEM measurements to determine the surface morphologies of the 80 nm thick C_{60} films, which were deposited on the STO/LSMO to mimic their growth as in our actual organic SV devices, as shown in Figure 6. From Figure

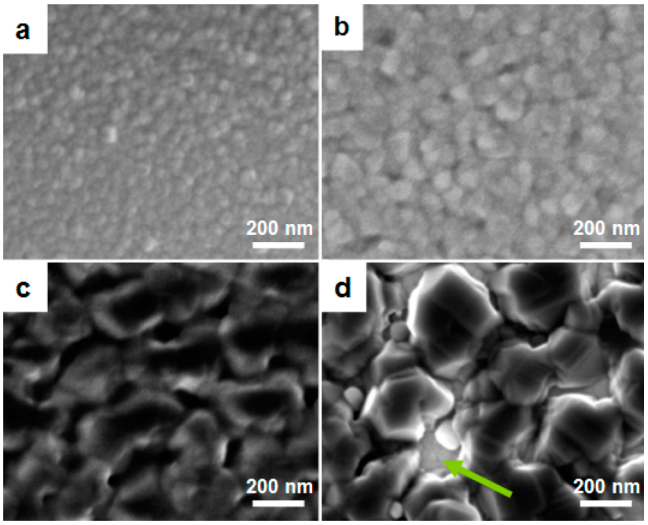

Figure 6. SEM images of C_{60} films that were fabricated at substrate temperatures of (a) 25, (b) 50, (c) 100, and (d) 150 °C. The scale bar in each panel is 200 nm.

6a, the morphology of the film deposited at a substrate temperature of 25 °C is very smooth, whereas for the film which was deposited at a substrate temperature of 25 °C (Figure 6d), the surface morphology is very rough.

Furthermore, we then performed AFM measurements to determine the surface morphology of the C_{60} films with a thickness of 80 nm. Figure 7a shows the typical surface topographic image of the 80 nm C_{60} layer grown on the LSMO at a substrate temperature of 25 °C with the scanning size of 2 × 2 μm^2, and its section image is shown in Figure 7b. The film displays a homogeneous surface, and the surface morphology of the film is very smooth. The root mean squared (RMS) roughness is 0.68 ± 0.002 nm. The RMS roughness is independent of the film thicknesses (80 nm) and is consistent with a molecular size of C_{60} of around 1 nm. Because of the low roughness and high smoothness, the possible presence of pinholes and filament conduction channels within the C_{60} layers can be excluded. From the section image, it should also be noted that the maximum roughness is 4.32 nm, which is especially small compared with the thickness of the film of 80 nm.

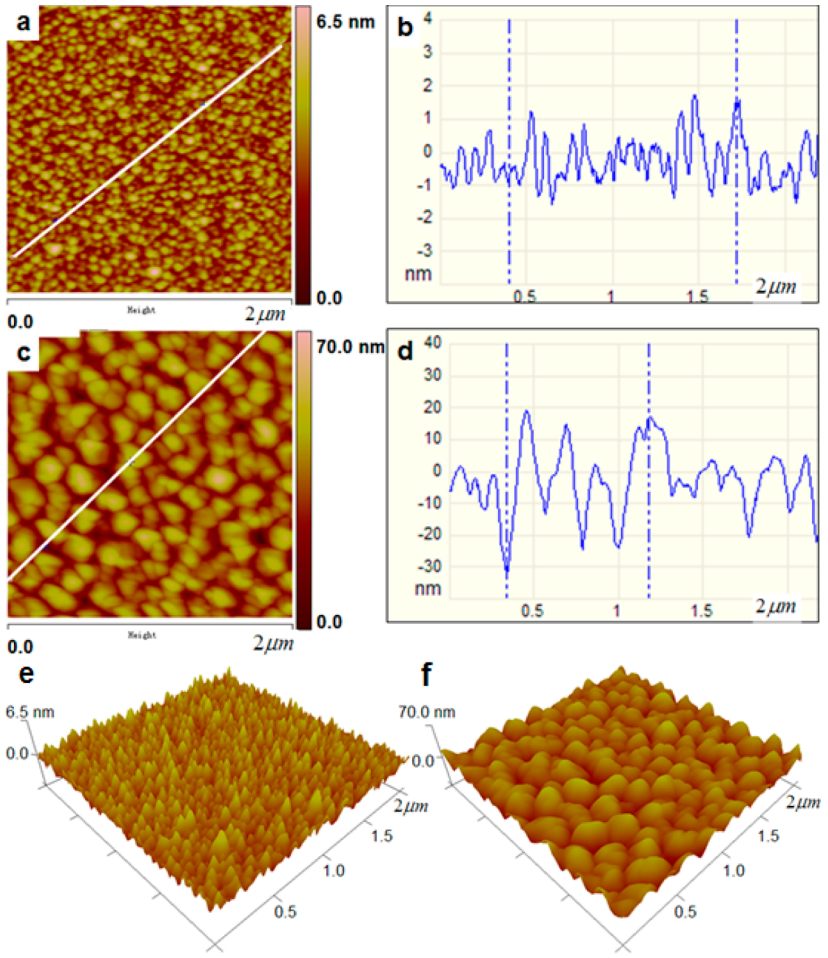

Figure 7. Atomic force microscopy (AFM) images of the C_{60} films deposited on LSMO at substrate temperatures of (a) 25 and (c) 150 °C. The profile along the lines highlighted in panels a and c are shown in panels b and d, respectively. (e, f) Three-dimensional AFM image of th eC_{60} film in panels a and c, respectively.

The typical surface morphology and its section information of the C_{60} film prepared at a substrate temperature of 150 °C are shown in Figure 7c, and the scanning size is also 2 × 2 μm^2. It can be seen that the surface of the film is not smooth but is uniform and continuous with many bigger nanocrystallines. In contrast, the faceted crystalline C_{60} film deposited at a substrate temperature of 150 °C exhibits a very rough surface morphology. The average grain size increases upon increasing the annealing temperature. The AFM images reveal that high temperatures support the crystallization of the C_{60} molecules. Figure 4 presents the XRD patterns of the C_{60} thin films deposited at substrate temperatures of 25−150 °C. The C_{60} films subjected to the lower substrate temperature possess amorphous features, whereas those deposited at a substrate temperature of 150 °C exhibit strong diffraction peaks of crystalline C_{60}. However, the C_{60} molecule is the typical spherical molecule, so when the C_{60} film was prepared at a higher substrate temperature, the grain size would become larger accordingly, and the pronounced grain-boundary effects become apparent, resulting in many tiny protuberances (light areas) and some pits (dark areas) on the surface of the film (Figure 7f). The height of the protuberances and the deepness of the pinholes can be seen from the section images, and the maximum values are about 25 and 35 nm, respectively. The RMS roughness of the surface is 8.28 nm. The more intuitive 3D AFM images (2 × 2 μm^2) of the C_{60} films, deposited at substrate temperatures of 25 and 150 °C, are shown in Figure 7 panels e and f, respectively, which provide more details on the plane areas. Obviously, from Figure 7f, the surface is composed of relatively large uniform nanocrystallines, and the pits and hollows with vertical deepness of about more than 60 nm spread over the scanning size of the film. These pits and hollows on the surface of the C_{60} films may lead to the formation of an ill-defined layer in organic spin valves. It is not difficult to understand that if the effective organic semiconductor interlayer is not thick enough, then the top Co impurities, which penetrate into and fill in these pits and hollows during magnetic metallic electrode deposition, will be very close and will even contact with the LSMO film so that the organic spin valves will form the spin-polarized tunneling channels and will be short cut. Therefore, the especially large MR data obtained for the C_{60}-based SV device in which the C_{60} interlayer was deposited at the substrate temperature of 150 °C should originate from the tunneling behavior of spin-polarized carriers through the C_{60} spacer with many pits and hollows on the surface of it. More work will be performed on controlling the crystallinity of the C_{60} films and thus the carrier mobility using some other effective methods to elucidate the relationship among the carrier transport, MR values, and spin diffusion length of the C_{60} SVs.

CONCLUSIONS

We have prepared vertical LSMO/C_{60}/Co SV devices all having the same thick C_{60} spacers that were deposited at different substrate temperatures. The interesting larger value of the MR ratio was observed in the device with a C_{60} spacer prepared at a higher substrate temperature. The detailed MR curves and $I-V$ characterizations of the devices indicate a transition of the spin transport behavior from spin injection and hopping transport inside the C_{60} spacer, which were deposited at low substrate temperatures, into tunneling through the C_{60} layer prepared at high substrate temperatures. The SEM and AFM measurements further illustrate that the occurrence of pits and hollows on the surface of C_{60} spacer deposited at the higher substrate temperatures will cause the formation of spin-tunneling channels in the vertical C_{60}-based SV devices.

AUTHOR INFORMATION

Corresponding Author

*E-mail: lfeng99@mail.ustc.edu.cn.

Notes

The authors declare no competing financial interest.

REFERENCES

(1) Naber, W. J. M.; Faez, S.; van der Wiel, W. G. *J. Phys. D: Appl. Phys.* **2007**, *40*, R205−R228.
(2) Nguyen, T. D.; Hukic-Markosian, G.; Wang, F.; Wojcik, L.; Li, X.; Ehrenfreund, E.; Vardeny, Z. V. *Nat. Mater.* **2010**, *9*, 345−352.
(3) Xiong, Z. H.; Wu, D.; Vardeny, Z. V.; Shi, J. *Nature* **2004**, *427*, 821−824.
(4) Dediu, V.; Hueso, L. E.; Bergenti, I.; Riminucci, A.; Borgatti, F.; Graziosi, P.; Newby, C.; Casoli, F.; De Jong, M. P.; Taliani, C.; Zhan, Y. *Phys. Rev. B* **2008**, *78*, 115203-1−115203-6.
(5) Wang, F. J.; Yang, C. G.; Vardeny, Z. V.; Li, X. G. *Phys. Rev. B* **2007**, *75*, 245324-1−245324-7.
(6) Dediu, V. A.; Hueso, L. E.; Bergenti, I.; Taliani, C. *Nat. Mater.* **2009**, *8*, 707−716.
(7) Mooser, S.; Cooper, J. F. K.; Banger, K. K.; Wunderlich, J.; Sirringhaus, H. *Phys. Rev. B* **2012**, *85*, 235202-1−235202-7.
(8) Santos, T. S.; Lee, J. S.; Migdal, P.; Lekshmi, I. C.; Satpati, B.; Moodera, J. S. *Phys. Rev. Lett.* **2007**, *98*, 016601-1−016601-4.
(9) Barraud, C.; Seneor, P.; Mattana, R.; Fusil, S.; Bouzehouane, K.; Deranlot, C.; Graziosi, P.; Hueso, L.; Bergenti, I.; Dediu, V.; Petroff, F.; Fert, A. *Nat. Phys.* **2010**, *6*, 615−620.
(10) Szulczewski, G.; Tokuc, H.; Oguz, K.; Coey, J. M. D. *Appl. Phys. Lett.* **2009**, *95*, 202506-1−202506-3.
(11) Yoo, J. W.; Jang, H. W.; Prigodin, V. N.; Kao, C.; Eom, C. B.; Epstein, A. J. *Phys. Rev. B* **2009**, *80*, 205207-1−205207-9.
(12) Lin, R.; Wang, F.; Rybicki, J.; Wohlgenannt, M.; Hutchinson, K. A. *Phys. Rev. B* **2010**, *81*, 195214-1−195214-6.
(13) Xu, W.; Szulczewski, G. J.; LeClair, P.; Navarrete, I.; Schad, R.; Miao, G.; Guo, H.; Gupta, A. *Appl. Phys. Lett.* **2007**, *90*, 072506-1−072506-3.
(14) Vinzelberg, H.; Schumann, J.; Elefant, D.; Gangineni, R. B.; Thomas, J.; Buchner, B. *J. Appl. Phys.* **2008**, *103*, 093720-1−093720-5.
(15) Majumdar, S.; Majumdar, H. S.; Laiho, R.; Osterbacka, R. *New J. Phys.* **2009**, *11*, 013022.
(16) Wang, F.; Vardeny, Z. V. *Synth. Met.* **2010**, *160*, 210−215.
(17) Gobbi, M.; Golmar, F.; Llopis, R.; Casanova, F.; Hueso, L. E. *Adv. Mater.* **2011**, *23*, 1609−1613.
(18) Tran, T. L. A.; He, T. Q.; Sanderink, J. G. M.; van der Wiel, W. G.; de Jong, M. P. *Adv. Funct. Mater.* **2012**, *22*, 1180−1189.
(19) Lin, R.; Wang, F.; Wohlgenannt, M.; He, C.; Zhai, X.; Suzuki, Y. *Synth. Met.* **2011**, *161*, 553−557.
(20) Zhang, X.; Mizukami, S.; Kubota, T.; Ma, Q.; Oogane, M.; Naganuma, H.; Ando, Y.; Miyazaki, T. *Nat. Commun.* **2012**, *4*, 1392.
(21) Akerman, J. J.; Escudero, R.; Leighton, C.; Kim, S.; Rabson, D. A.; Dave, R. W.; Slaughter, J. M.; Schuller, I. K. *J. Magn. Magn. Mater.* **2002**, *240*, 86−91.